and defect dependence of the etching rate. They explain the large differences in the surface morphology generated by different etchants.

REFERENCES

1. W. Kern, in "Etching for Pattern Definition," H. G. Hughes and M. J. Rand, Editors, p. 1, The Electrochemical Society Softbound Proceedings Series, Princeton, NJ (1976).
2. B. L. Sopori, *This Journal*, **131**, 667 (1984).
3. H. Gerischer, *ibid.*, **113**, 1174 (1966).
4. D. R. Turner, *ibid.*, **107**, 810 (1960).
5. R. Memming and G. Schwandt, *Surf. Sci.*, **4**, 109 (1966).
6. M. Matsumura and R. S. Morrison, *J. Electroanal. Chem.*, **144**, 113 (1983); *ibid.*, **147**, 157 (1983).
7. H. Gerischer and M. Lübke, *Ber. Bunsenges. Phys. Chem.*, **91**, 394 (1987).
8. H. Gerischer and F. Beck, *Z. Phys. Chem., Frankfurt*, **13**, 389 (1957).
9. H. Gerischer and I. Wallem-Mattes, *ibid., Frankfurt*, **64**, 187 (1969).
10. B. R. Weinberger, G. G. Peterson, T. C. Eschrich, and H. A. Krasinski, *J. Appl. Phys.*, **60**, 3232 (1986).
11. R. E. White and S. E. Lorimer, *ibid.*, **130**, 1096 (1983).
12. M. Magistragostino and C. Gramellini, *Electrochim. Acta*, **30**, 373 (1985).

A Mathematical Model for a Parallel Plate Plasma Etching Reactor

Demetre J. Economou[*,1] and Richard C. Alkire[*]

Department of Chemical Engineering, University of Illinois at Urbana-Champaign, Urbana, Illinois 61801

ABSTRACT

A mathematical model was formulated for predicting species concentration profiles and etch rate distribution in a parallel plate plasma reactor. Explicit account was taken of the ion-assisted component of etching by considering ion transport in the sheath. For the case of oxygen discharge, convective diffusion and chemical reactions of the etchant species were included as well as the electron density and energy variations in the bulk plasma. Important dimensionless system parameters were identified and their effect on etch rate, degree of etch anisotropy, and uniformity was examined. The model predictions were evaluated by comparison with experimental data on etch rate of polymer in an oxygen plasma as a function of pressure, power, and flow rate. For each, the model captured the salient features observed experimentally, although quantitative comparisons were not possible owing to the lack of accurate rate reaction kinetics data.

The central goal of patterning by plasma processing is to obtain high etch rate while at the same time preserving anisotropy, uniformity, and selectivity. Significant advances in fundamental understanding of plasma-assisted processes have been reported in the recent past (1), although engineering development of new systems continues to rely heavily upon trial-and-error procedures. In the present work, a reactor engineering approach is described for simulating plasma etching in a parallel plate reactor.

There have recently been several noteworthy investigations aimed at modeling plasma processes. Allen *et al.* (2) used simplified models and a variety of experimental techniques to predict etch rate and anisotropy of polysilicon etching. Kushner (3), emphasized the discharge chemistry whereas Graves and Jensen (4) emphasized the discharge structure. In these works the variation of etch uniformity along the wafer was not addressed.

Other investigators emphasized transport and reaction phenomena in systems where ion-assisted chemistry was relatively unimportant. Dalvie *et al.* (5) studied etching uniformity in a Reinberg-type reactor. Edelson and Flamm (6) and Kline (7) presented plug flow reactor models including relatively detailed chemical reaction schemes. Diffusion and reaction in barrel etchers were studied by Alkire and Economou (8), Doken and Miyata (9), and others. In these works ion transport and etch anisotropy were not considered.

Etching in oxygen plasmas has been cited by De Graff and Flanders (10) as "an excellent model system for studying etching of materials in reactive gases . . . ." There is extensive information on the oxygen discharge (11, 12) and reactor models for producing O-atoms from flowing O_2 discharges have been reported (13).

In the present work, a plasma reactor engineering model was developed based on potential field, transport and reaction principles. Ion-assisted etching was accounted for by including consideration of both ion transport in the sheath region, and the effect of ion flux on surface reaction rates. The oxygen discharge etching of polymer was chosen as a model system for experimental study.

Theoretical

The plasma reactor to be modeled, depicted in Fig. 1, consists of two parallel disk-shaped electrodes separated by a distance of 2L, with the wafer resting on the grounded electrode. Gas is continuously fed through portholes in the upper electrode. Reaction products and unreacted species are pumped radially outwards to the exit. Typical parameter values for the system used in the present work are given in Table I.

The following paragraphs summarize salient features of the phenomena which occur in the glow and sheath regions, the transport processes, and reaction sequences.

The glow (bulk plasma) region.—The glow region was assumed to resemble a positive column (14) because, at the high frequencies ($\gtrsim$ 10 MHz) and pressures ($\sim$ 1 torr) of interest in single-wafer etching, bulk ionization dominates over ionization by secondary electrons. Further, the secondary electron yield of molecular ions is very low.

The effective electric field (12, 14) is the steady dc field which would couple the same energy to the electrons as the actual high frequency field. In the present work, the effective-electric-field-to-pressure ratio E_{ef}/p for the oxygen plasma was taken from Fig. 1.19 of Bell (12) where E_{ef}/p is plotted against the product of pressure (p) and electron diffusion length (Λ) for a diffusion-controlled discharge. That plot was derived from data on pure oxygen. In the present work, it was assumed that the exposed polymer area is small and the gas flow rate is high so that the etching product (CO_2, CO, H_2O) concentrations are small, *i.e.*, the ratio
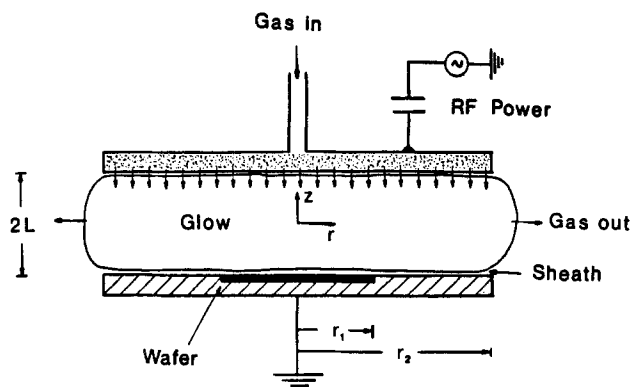
Fig. 1. Schematic of the parallel plate plasma reactor studied

$R_t A_{PR}/Q_o C_o \ll 1$, and the discharge behaves as though it were one in pure oxygen (15). Here, R_t is the total etch rate, A_{PR} is the exposed polymer area, and $Q_o C_o$ is the feed gas molar flow rate. For typical parameter values (Table I) the above ratio has a value of 0.025. Moreover E_{ef}/p was assumed spatially uniform in the bulk plasma. After having found E_{ef}/p, average electron energy and electron transport and reaction coefficients may be determined for processes with known cross section.

Modulation of the electron energy distribution function may invalidate the effective electric field, E_{ef}, approximation. The degree of modulation depends on the electron energy-exchange frequency $\nu_u = u_{de}E/\xi_k$, where u_{de} is the electron drift velocity and ξ_K is the characteristic energy of the electrons. When $\nu_u > \omega$, where ω is the applied radian frequency, modulation of the distribution function is significant. Under typical conditions for the system at hand (Table I), ν_u was found to be 48 MHz, about 3.5 times greater than the applied frequency of 13.56 MHz. Hence some modulation of the electron energy may be expected. This in turn will lead to modulation of etchant production by electron impact dissociation. However, etchant losses (by etching reaction, convection, etc.) occur in a time scale much longer than etchant production. Therefore, the etchant concentration should not be modulated in time. Further, in a study by Rogoff et al. (16), the instantaneous plasma electric field was calculated for a 13.56 MHz, relatively high pressure (~ 1 torr) Cl_2 bulk plasma. The results were compared with the effective field approximation. It was found that E_{ef} represented well the power input to the plasma, although there was a 30% discrepancy in the value of E/N required to sustain the discharge. It appears that the effective field approach is quite reasonable for the high frequency discharges, especially for simplified discharge models such as the model used in the present work. The effective field approximation may not be accurate, however, for the low frequency discharges (<10 MHz).

The sheath region.—The present work emphasizes applications at 13.56 MHz. At such high frequency, ions respond to a time-average dc sheath voltage. The drift velocity of the ions was determined by coupling the equations of current continuity and ion motion to Poisson's equation for the potential distribution in the sheath. Of the various possible ionic species, the sheath was assumed to contain only positive ions, namely, O_2^+. Elastic hard-sphere and charge-exchange collisions of ions with neutrals were accounted

Table I. Typical parameter values for system studied

Symbol	Name	Value
L	Half interelectrode gap	1.10 cm
P	Power	100W
p	Pressure	1 torr
Q	Gas flow rate under plasma reactor conditions	1623 cm³/s
Q_o	Inlet gas flow rate	100 sccm
r_1	Wafer radius	3.80 cm
r_2	Reactor radius	7.30 cm
τ_g	Mean gas residence time	0.227s
ω	Applied frequency	13.56 MHz

for by a "frictional" force opposing the ion motion. Collision dynamics considerations revealed that in the limit of high ion kinetic energy compared to thermal energy (a condition readily satisfied in the sheath), the frictional force was proportional to the square of the ion drift velocity. The dimensionless quantity $Co = 1/2\ \sigma_t N\lambda_D$ (collision number) was found to be important in describing the ion motion in the sheath. Here σ_t is the total ion-molecule collision cross section, N is the gas density, and λ_D is the Debye length. An analytic expression for the ion bombardment energy was derived, in terms of Co and the sheath voltage, for the range of parameter values typical of high pressure (~ 1 torr) diode plasma etching. The sheath model provided the energy and flux of ions bombarding the substrate as a function of reactor operating pressure and power. Such quantities were used along with a kinetic expression in the plasma reactor model to calculate etch rate and anisotropy. Details about the sheath model have been reported elsewhere (17).

Transport and reaction phenomena.—In order to simplify the analysis, only the species which were thought to be most important for the system at hand were considered. Dettmer (11) and Thompson (18) found O_2^+ and O^- to be the dominant positive and negative ions, respectively. For $p \gtrsim 1$ torr and $E/N \gtrsim 50$ Td (conditions typical for the system at hand), Dettmer found the negative ion concentration in the bulk plasma to be small compared to the electron concentration. Therefore, the electron and positive ion density nearly balance each other. The only neutrals considered were atomic and molecular oxygen.

The electron balance was considered first. Electrons are generated in the bulk plasma mainly by reactions such as [See Ref. (11, 12)]

Ionization

$$O_2 + e \rightarrow O_2^+ + 2e \qquad [R1]$$
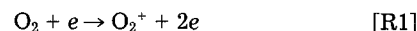
Metastable (two-step) ionization

$$O_2(^1\Delta_g) + e \rightarrow O_2^+ + 2e \qquad [R2]$$
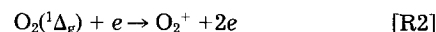
Detachment from O-atoms

$$O + O^- \rightarrow O_3 + e \qquad [R3]$$

Detachment by metastable oxygen

$$O_2(^1\Delta_g) + O^- \rightarrow O_2 + e \qquad [R4]$$
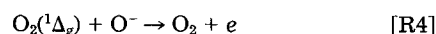
and are eliminated mainly by diffusion and reactions such as

Attachment to O_2

$$O_2 + e \rightarrow O + O^- \qquad [R5]$$

Attachment to metastable oxygen

$$O_2(^1\Delta_g) + e \rightarrow O + O^- \qquad [R6]$$
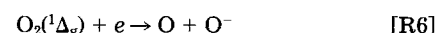
Attachment and detachment reactions nearly balance each other (11). Hence the electron balance will be dominated by ionization and diffusion (diffusion-controlled discharge).

The assumption of ambipolar diffusion (19) yields

$$D_a\nabla^2 n_e + K_i n_e = 0 \qquad [1]$$

where D_a is the ambipolar diffusion coefficient, n_e is the electron density, and K_i is an effective ionization coefficient accounting for all the electron producing reactions which are linear in electron density. Equation [1] neglects convection of electrons by bulk gas flow as compared to ambipolar diffusion. This is reasonable since the corresponding Peclet number was estimated to be less than 0.01. Boundary conditions for Eq. [1] include zero electron concentration on the walls (Eq. [2]), and the symmetry condition (Eq. [3])

$$n_e = 0 \text{ at } z = \pm L \text{ and at } r = r_2 \qquad [2]$$

$$\frac{\partial n_e}{\partial r} = 0 \text{ at } r = 0 \text{ and } \frac{\partial n_e}{\partial z} = 0 \text{ at } z = 0 \qquad [3]$$

The solution for the dominant (lowest) mode of diffusion is (14)

$$n_e(\xi, \zeta) = n_{eo} J_o (2.405\xi) \cos\left(\frac{\pi}{2}\zeta\right) \qquad [4]$$

Under the conditions of ambipolar diffusion $n_+ \simeq n_e$ and therefore Eq. [4] provides the bulk plasma positive ion density profile as well. Substitution of Eq. [4] into Eq. [1] yields the condition for a self-sustained discharge

$$\frac{1}{\Lambda^2} = \frac{K_i}{D_a} = \left(\frac{2.405}{r_2}\right)^2 + \left(\frac{\pi}{2L}\right)^2 \qquad [5]$$

where Λ is the electron diffusion length, and r_2 is the reactor radius.

The electron density at the reactor center (n_{eo}) was determined by the power input to the system. The main plasma body is resistive in nature and current in the plasma is carried by electrons. The power dissipated per unit plasma volume is

$$P/v_p = \frac{n_{av}e^2 E_{ef}^2}{m v_e} \qquad [6]$$

where n_{av} is the average electron density, m is the electron mass, and v_e is the electron momentum transfer collision frequency. Bell showed that the expression $v_p n_{av}/(P\Lambda)$ is a function of $p\Lambda$ only and gave a plot corresponding to the oxygen discharge [Fig. 1.19 of Bell (12)]. Such data were used in the present study for finding the average electron density n_{av}, given the reactor pressure p, geometry (Λ), and power input per unit volume P/v_p.

The atomic oxygen material balance is

$$U \frac{dC_1}{dr} = D_1 \left[\frac{1}{r}\frac{d}{dr}\left(r\frac{dC_1}{dr}\right)\right] + G_1 \qquad [7]$$

where C_1 is the atomic oxygen concentration and U is the radial gas flow velocity averaged over the axial (z) dimension. Equation [7] represents a one-dimensional radial dispersion model (20). Axial concentration gradients were neglected owing to the large aspect ratio of the reactor r_2/L. Further, the dispersion coefficient equals the molecular diffusivity (D_1) at the low pressure used. The radial gas flow velocity was obtained by a macroscopic mass balance as $U = Qr/(4\pi L r_2^2)$ where Q is the gas flow rate and r is the radial coordinate. One observes that the radial velocity is zero at the reactor center, increases linearly with radial position, and is maximum at the reactor exit. The gas flow rate was corrected for changes (from input conditions) in gas temperature and pressure by assuming ideal gas behavior. The diffusivity of O-atoms in O_2 was determined by using the experimental value of the collision diameter σ_{12} for O-O_2 equal to 3.12Å.

Atomic oxygen is produced by dissociation of molecular O_2, and is eliminated by etching, surface recombination, and volume recombination reactions. The net generation term was thus written as

$$G_1 = 2k_p C_2 n_e - \frac{1}{2L}(R_n + R_+) - \frac{v_o w_1}{8L}C_1$$

$$- \frac{v_o w_2}{8L}C_1 - (K_1 C_1^2 C_2 + K_2 C_1^3 + K_3 C_1 C_2^2) \qquad [8]$$

where C_2 is the molecular oxygen concentration. The first term on the right-hand side (rhs) of Eq. [8] gives the production of atomic oxygen by electron impact dissociation of molecular oxygen

$$O_2 + e \xrightarrow{k_p} 2O + e \qquad [R7]$$
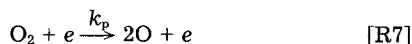
Kaufman (15) showed Eq. [R7] to be the main O-atom production channel. The second term on the rhs of Eq. [8] represents the kinetics of the etching reaction. Since etching is a surface reaction, the surface to volume ratio $1/2L$

was used to transform to a pseudo-volumetric reaction term for the one-dimensional model.

In this work, the total etch rate was assumed to be the sum of two contributions: chemical etching (R_n) arising from the spontaneous reaction of O-atoms with the film, and ion-assisted etching (R_+) due to reactions caused by ion bombardment

$$R_t = R_n + R_+ \qquad [9]$$

The contribution of a third component, sputtering, was neglected. The kinetics of etching are poorly understood. The decoupling of the total etch rate into chemical and ion-assisted components has been used in connection with ion beam studies of the Si/XeF_2 system (21). Such a decoupling was discussed later by Winters and Coburn (22). However, Lee and Chen (23) experimentally separated the total etch rate into chemical and ion-assisted components under actual plasma etching conditions (Si/F-atoms system). Such an additive model was also used by Allen *et al.* (2) to describe silicon etching in CF_3Cl/Ar plasmas.

For the chemical etching component linear kinetics was assumed to apply, $R_n = k_n C_1$. Such kinetics has been observed for systems such as photoresist/O-atoms (24, 25) and Si or SiO_2/F-atoms (26). Ion-assisted etching kinetics is more complicated. The expression $R_+ = k_+ I_+ \epsilon_+$ was used, suggesting that ion-assisted etching is proportional to the power deposited on the surface by the bombarding ions. Here I_+ and ϵ_+ are the positive ion bombardment flux and energy, respectively, and k_+ is the corresponding reaction rate constant. The total etch rate was then taken as

$$R_t = k_n C_1 + k_+ I_+ \epsilon_+ \qquad [10]$$

More complex surface kinetics could be used, but that would introduce additional unknown kinetic parameters. When Eq. [10] was applied for the conditions used by Lee and Chen (23), *i.e.*, no ion collisions in the sheath and strongly asymmetric system so that the sheath voltage equals the self-bias voltage, Eq. [4] of their paper was recovered. The degree of etch anisotropy, excluding ion divergence effects was defined as

$$An = R_+/(R_+ + R_n) \qquad [11]$$

This definition of anisotropy is more appropriate at lower pressure at which ion transport in the sheath is anisotropic (*e.g*, negligible ion-neutral collisions randomizing the ion motion). When $R_+ >> R_n$, anisotropic profiles with minimum undercut may be expected.

The third term on the right-side of Eq. [8] represents electrode surface (wall) recombination of atoms. Here v_o is the random thermal velocity of atomic oxygen, w_1 is the wall recombination coefficient of the substrate electrode, and w_2 is the wall recombination coefficient of the counter-electrode. The wall recombination rate was obtained by multiplying the random flux of the O-atoms to the surface ($1/4\, v_o C_1$) by the surface to volume ratio ($1/2L$) and by the corresponding wall recombination coefficient w_i ($i = 1,2$). The wall recombination coefficient is critically dependent on the nature of the surface.

The last term in parentheses on the right-hand side of Eq. [8] represents volume recombination of O-atoms which occurs according to

$$2\,O + O_2 \xrightarrow{K_1} 2\,O_2 \qquad [R8]$$

$$3\,O \xrightarrow{K_2} O_2 + O \qquad [R9]$$

$$O + 2\,O_2 \xrightarrow{K_3} O_3 + O_2 \qquad [R10]$$
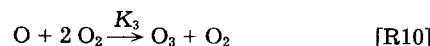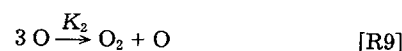
Volume recombination reactions are strongly dependent on pressure (rate proportional to p^3) and are normally negligible for pressures less than 1 torr.

Combining Eq. [7], [8], and [10] one obtains

$$\frac{Qr}{4\pi L r_2}\frac{dC_1}{dr} = D_1\left[\frac{1}{r}\frac{d}{dr}\left(r\frac{dC_1}{dr}\right)\right] + 2k_p C_2 n_e$$

$$-\frac{1}{2L}(k_n C_1 + k_+ I_+ \epsilon_+) - \frac{v_o w_1}{8L}C_1$$

$$-\frac{v_o w_2}{8L}C_1 - (K_1 C_1{}^2 C_2 + K_2 C_1{}^3 + K_3 C_1 C_2{}^2) \quad [12]$$

Boundary conditions to Eq. [12] include

$$\frac{dC_1}{dr}\Big|_{r=0} = 0 \text{ and } C_1|_{r=r_2} = C_{ex} \quad [13]$$

with the exit concentration adjusted so that the overall mass balance is obeyed

$$2L\int_0^{r_2}(2k_p C_2 - C_1)\, n_e 2\pi r dr = \int_0^{r_1}(k_n C_1 + k_+ I_+ \epsilon_+)\, 2\pi r dr$$

$$+ \int_0^{r_2}\frac{v_o}{4}(w_1 + w_2)\, C_1 2\pi r dr + 2L\int_0^{r_2}(K_1 C_1{}^2 C_2 + K_2 C_1{}^3$$

$$+ K_3 C_1 C_2{}^2)\, 2\pi r dr + Q C_{ex} \quad [14]$$

A separate material balance for O_2 is not required since

$$C_R = C_1 + C_2 = \frac{p}{R_g T_g} \quad [15]$$

where T_g is the gas temperature and R_g is the universal gas constant.

Equations [12]-[15] were converted to dimensionless form by defining

$$\theta_1 = \frac{C_1}{C_R} \quad \xi = \frac{r}{r_2} \quad C_R = \frac{p}{R_g T_g} \quad \theta_e = \frac{n_e}{n_{av}} = 2.316\, J_o(2.405\xi) \quad [16]$$

$$\epsilon_+{}^* = \frac{\epsilon_+}{eV_s} \quad I_+{}^* = \frac{I_+}{n_+ u_R} \quad \text{with } u_R = \sqrt{2kT_e/M_2} \quad [17]$$

Here, V_s is the sheath voltage, n_+ is the positive ion density in the bulk plasma, and M_2 is the $O_2{}^+$-ion mass.

Upon substitution into Eq. [12]

$$Pe\,\xi\frac{d\theta_1}{d\xi} = \frac{d^2\theta_1}{d\xi^2} + \frac{1}{\xi}\frac{d\theta_1}{d\xi} + Da\,\theta_e(1 - \theta_1)$$

$$-(\Phi_o{}^2\theta_1 + \delta\Phi_o{}^2\theta_e I_+{}^*\epsilon_+{}^*) - (\gamma_1 + \gamma_2)\theta_1 - \beta_3\theta_1$$

$$-(\beta_1 - 2\beta_3)\theta_1{}^2 - (\beta_2 + \beta_3 - \beta_1)\theta_1{}^3 \quad [18]$$

where the dimensionless parameters were defined as

$$Pe = \frac{Q}{4\pi L D_1} \quad \Phi_o{}^2 = \frac{k_n r_2{}^2}{2L D_1} \quad Da = \frac{2k_p r_2{}^2 n_{av}}{D_1} \quad [19]$$

$$\beta_i = \frac{K_i C_R{}^2 r_2{}^2}{D_1}(i = 1, 2, 3)$$

$$\gamma_1 = \frac{v_o w_1 r_2{}^2}{8L D_1} \quad \gamma_2 = \frac{v_o w_2 r_2{}^2}{8L D_1} \quad \delta = \frac{k_+ n_{av}(eV_s)\, u_R}{k_n C_R} \quad [20]$$

The expression for θ_e in Eq. [16] resulted from averaging Eq. [4] over the axial coordinate. The boundary conditions became

$$\frac{d\theta_1}{d\xi}\Big|_{\xi=0} = 0 \qquad \theta_1|_{\xi=1} = \theta_{ex} \quad [21]$$

The dimensionless overall mass balance became

$$\int_0^1 [Da(1 - \theta_1)\theta_e - (\gamma_1 + \gamma_2)\theta_1 - \beta_3\theta_1$$

$$-(\beta_1 - 2\beta_3)\theta_1{}^2 - (\beta_2 + \beta_3 - \beta_1)\theta_1{}^3]\xi d\xi$$

$$= \int_0^{\xi_1} \Phi_o{}^2(\theta_1 + \delta\theta_e I_+{}^*\epsilon_+{}^*)\, \xi d\xi + Pe\, \theta_{ex} \quad [22]$$

where

$$\xi_1 = \frac{r_1}{r_2} \text{ and } \theta_{ex} = \frac{C_{ex}}{C_R} \quad [23]$$

The Peclet number, Pe, characterizes the relative importance of etchant convection and diffusion. For high flow rates and/or low diffusivities (high Pe) convection dominates (e.g., plug flow reactor); for low Pe, backmixing dominates, reducing concentration gradients. The Thiele modulus $\Phi_o{}^2$ describes the effect of chemical etching as compared to diffusion. Large values of $\Phi_o{}^2$, such as under rapid chemical reaction or slow diffusion, would create large concentration gradients across the reactor. On the other hand, small values of $\Phi_o{}^2$ imply rapid diffusion which, in the absence of other effects, tends to render concentration profiles uniform. The Damköhler number, Da, relates volume production to diffusion. If Da is large, etchant species are produced faster than they can diffuse, and large concentration gradients may develop.

Dimensionless groupings β_i ($i = 1, 2, 3$) describe volume recombination vs. diffusion effects and are of secondary importance at low pressures but may become important at higher pressure ($\gtrsim 1$ torr). Groupings γ_1 and γ_2 are similar to the Thiele modulus but with the surface recombination reaction rate constant replacing the chemical etching rate constant. Finally, dimensionless grouping δ characterizes the degree of etch anisotropy. Large values of δ would result in anisotropic etching such as for rapid ion-assisted reactions (large k_+), large electron (and thus positive ion) densities, n_{av}, large sheath voltages, V_s, for slow chemical etching (small k_n), and low pressure (small C_R). Hence by manipulating reactor variables so as to vary the value of δ from small to large, etching profiles can be varied between isotropic and anisotropic profiles (23, 27). It should be noted here that the characteristic length used in the relevant dimensionless groupings is the reactor radius r_2, a choice that is consistent with the use of a radial dispersion model.

The etching reaction rate constants and the wall recombination coefficients were unknown so that estimated quantities had to be used. The chemical etching rate constant was estimated from experimental data on the loading effect (28). The ion-assisted etching rate constant was estimated from SEM photographs of the cross section of features etched under low pressure conditions for which ion-assisted etching occurs only in the vertical direction. Finally, the wall recombination coefficient may be estimated from experimental data of O-atom concentration in the absence of etchable material.

Method of solution.—Solution to Eq. [18] subject to boundary conditions Eq. [21] and [22] gave the concentration distribution of the etchant species along the wafer surface. Also obtained were the etch rate distribution, and the degree of etch anisotropy as a function of reactor operating conditions.

Two methods of solution were used. First, the model equations were solved by prescribing values to the dimensionless groupings, and the effect of their variation on etch rate, etch uniformity, and degree of etch anisotropy was investigated. In this approach, Eq. [18] was solved by linearizing about a trial solution and using a finite difference scheme (32). After a convergent solution was obtained (within 0.01% of two successive concentration distributions) the concentration profile was used to evaluate the integrals of the overall mass balance, Eq. [22]. Calculations stopped when the overall mass balance was satisfied to within 0.1%. The number of radial grid points was typically 100. The values of $I_+{}^*$ and $\epsilon_+{}^*$ needed for integrating Eq. [18] were obtained by solving the sheath model equations at each point of the finite difference grid. A Runge-Kutta

method was used to integrate the initial value problem with respect to the sheath coordinate. Sheath calculations stopped when the electrode potential was reached. Details of the sheath calculations can be found elsewhere (17).

The second method of approach consisted of using numerical values of the dimensional quantities (power, pressure, flow rate, etc.) which corresponded to etching a novolak-type photoresist in an oxygen plasma. The purpose of these calculations was to compare theoretical predictions with experimental results obtained with the parallel plate reactor system described below.

Experimental

A schematic diagram of the experimental system is shown in Fig. 2. The 14.6 cm diam powered (13.56 MHz, Plasma Therm) showerhead electrode was surrounded by a Macor ceramic ring that served partially to confine the plasma. A groove was cut into the 10.2 cm diam grounded aluminum substrate electrode so that a 3 in. silicon wafer would be flush with the electrode surface. The interelectrode distance was 2.2 cm. Both electrodes were cooled (or heated) by a chiller/heater system (Bay Voltex). Gas pressure and flow rate were independently controlled with a closed-loop system (MKS Instruments). The RF voltage waveform and the self-bias voltage developed on the powered electrode were monitored during etching. The RF voltage was nearly sinusoidal. The dc self-bias voltage was close to zero at higher pressure for which the plasma was confined between the electrodes. Zero-grade oxygen gas was used for etching experiments (D&R Welding Supply); according to the gas supplier, the main impurities were N_2 (200 ppm), Ar (35 ppm), hydrocarbons (20 ppm), and H_2O (10 ppm). Most of the experimental runs utilized p-type (111), 3 in. diameter silicon wafers (2-4 Ω-cm resistivity) covered with a thin film of positive photoresist (Shipley 1400-33) having thickness in the range 1-4 μm. Etch rates of PR films were determined with a stylus profilometer (Alpha-Step Profiler, Tencor Instruments). The photoresist film used was a novolac resin with the following nominal composition by weight on a dry basis: 74% C, 16% O, 6% H, 2% N, and 2% S.

Results and Discussion

Results of the plasma reactor model are first presented in terms of important dimensionless parameters of the system.

Figure 3 shows the effect of Thiele modulus Φ_o^2 on the concentration distribution of etchant species θ_1 along the reactor radius ξ for typical parameter values. Note that $\Phi_o^2\delta$, which describes the effects of ion-assisted etching kinetics *vs.* diffusion, was kept constant as Φ_o^2 varied. The electron density distribution was assumed uniform (θ_e = 1). Volume recombination and wall recombination along the bottom electrode were neglected [$\beta_i = 0$ ($i = 1, 2, 3$), $\gamma_1 = 0$]. For small values of Φ_o^2, diffusion is facile and the reactant concentration over the etching surface is uniform. For large values of the Thiele modulus, chemical etching becomes an important sink of reactive species, and diffusion is not rapid enough to supply reactant from the relatively inert outer parts of the reactor ($\xi > 0.5$). Thus a "dip" in the concentration profile forms over the etching surface. Such dip in the etchant concentration profile has been re-
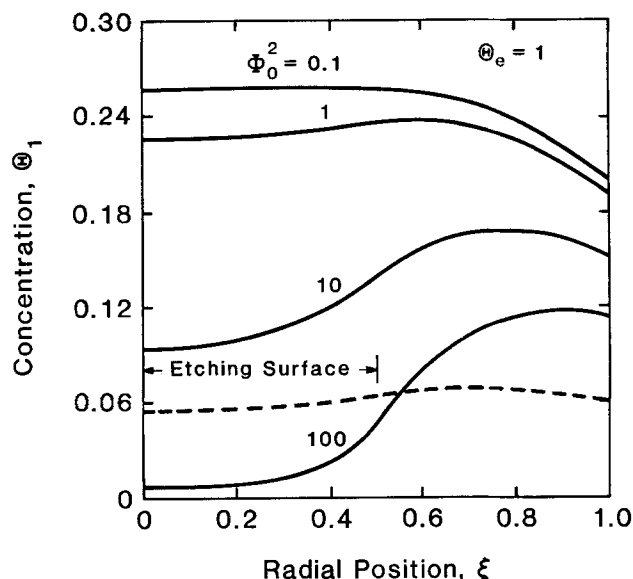
Fig. 3. Dimensionless etchant concentration as a function of radial position for different values of the Thiele modulus Φ_o^2. Co = Da = Pe = γ_2 = 1, $\Phi_o^2\delta$ = 5, $\gamma_1 = \beta_i$ = 0, V_p^* = -50, ξ_1 = 0.5, θ_e = 1. Dotted line shows the case γ_1 = 10, Φ = 10.

ported experimentally at boundaries where two surfaces having different etch rates met (29, 30). For the case under examination, ion-assisted etching was uniform over the etching surface since the electron (and hence the positive ion) density distribution was assumed uniform. Since chemical etching is proportional to reactant concentration, the concentration distribution provides a measure of etch uniformity. The profiles of Fig. 3 would give rise to the often observed "bullseye" wafer clearing pattern, in which etch rate decreases monotonically from the wafer periphery to its center.

Conditions which lead to large concentration gradients promote nonuniform etching and should thus be avoided. Etch uniformity can be improved by adjusting the reactivity of the surface surrounding the wafer, shown by the dashed curve in Fig. 3 which was computed for Φ_o^2 = 10 and γ_1 = 10. One observes that when the reactivity of the surface being etched is comparable to that of the surrounding surface, etch uniformity is greatly improved. Using a substrate electrode that etches as fast as the wafer itself (29), however, causes the etch rate to decrease be-

Fig. 2. Schematic diagram of the experimental system
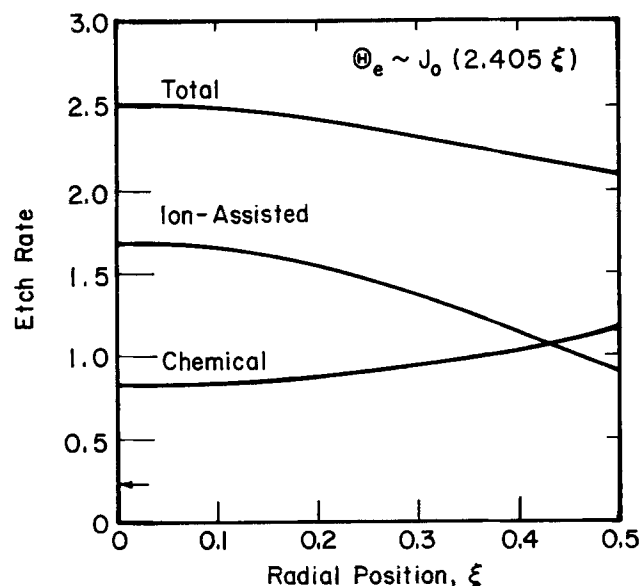
Fig. 4. Dimensionless etch rate as a function of radial position. Co = Da = Pe = γ_2 = 1, Φ_o^2 = 10, δ = 0.5, $\gamma_1 = \beta_i$ = 0, V_p^* = -50, ξ_1 = 0.5, θ_e = 2.316 J_o (2.405ξ).

cause the etchable surface area is larger (loading). This effect may be seen in Fig. 3 by the lower values of etchant concentration for $\gamma_1 = 10$ as compared to $\gamma_1 = 0$. If the Thiele modulus is very high (e.g., instantaneous etching reaction, $k_n \rightarrow \infty$), the etchant concentration on the surface will tend toward zero; the etching reaction will then be diffusion limited. Diffusion limitations are likely to become important as wafer (and reactor) size increases and as etching gas formulations are sought which provide faster etching rates (higher k_n).

The etch rate distribution may be quite different from the etchant concentration distribution when the electron (and therefore positive ion) density profile in the reactor is nonuniform. Figure 4 illustrates the situation for the case $\Phi_0^2 = 10$, $\delta = 0.5$; other parameter values are the same as in Fig. 3, expect that the electron density profile, no longer uniform, follows the Bessel function given by Eq. [16]. The dimensionless ion-assisted and chemical etching rates are defined as $R_+^* = \Phi_0^2\,\delta\epsilon_+{}^*I_+{}^*\theta_e$ and $R_n^* = \Phi_0^2\theta_1$, respectively (see also Eq. [18]). It may be seen that, although chemical etching is higher at the wafer edges, the total etch rate is higher at the center of the wafer because ion flux to the surface is higher there. Also seen in Fig. 4 is that the degree of etch anisotropy decreases towards the wafer edges. In order for both total etch rate and degree of anisotropy to be uniform across the wafer, both the chemical and the ion-assisted components of the etching process must be uniform.

The effect of flow velocity on the concentration distribution is seen in Fig. 5 for several values of the Peclet number. Note that the surface being etched extends from 0 to $\xi = 0.5$. At low Pe, diffusion is rapid and the concentration profiles tend to be uniform. Close to the reactor center, the local velocity is small (zero at the axis) and diffusion is rapid compared to convection, yielding more uniform concentration profiles. At low Pe the concentration distribution is determined by the reactivity of the surface rather than flow (the reactant residence time is long so that its effective lifetime is determined by chemical reaction). A "dip" in the concentration profile may then occur above the etching surface, as in Fig. 3. In such case the etching rate will be higher at the edge of the wafer (curve for Pe = 0.5 in Fig. 5). As Pe increases, reactant loss by convection increases yielding lower reactant concentration. At intermediate Pe the etching rate is uniform (curve for Pe = 1 in Fig. 5). As Pe increases further, the etching rate is higher at the wafer center (curve for Pe = 2, Fig. 5).

Although it is instructive to examine the effect each individual dimensionless group has on reactor performance, it is often the case that variation of one of the reactor operating variables affects a number of dimensionless groups simultaneously. Consider, for example, the consequence of changing reactor operating pressure. An increase in pressure (everything else held constant) has the following effect: (i) the effective electric-field-to-pressure ratio E_{ef}/p decreases, which in turn results in a decrease of the etchant production rate constant k_p; (ii) electron density n_{av} decreases (for $p \gtrsim 0.25$ torr) (12); (iii) electron energy (temperature T_e) decreases; (iv) molecular number density N increases leading to an increase in both C_2 and C_R; (v) reactant diffusivity decreases as does gas flow velocity. As a consequence, all dimensionless groups in Eq. [19] and [20] are affected except for the Peclet number. It is this complex interdependence of parameters that makes the task of predicting the behavior of plasma reactors invariably difficult.

Figure 6a shows experimental data for etch rate *vs.* pressure. At the higher pressures, the etch rate reached a maximum value and (not shown) then decreased at pressures above 2 torr.

Calculation of absolute etch rates requires knowledge of the etching reaction stoichiometry in addition to the etch rate constants. The reaction stoichiometry is unknown. The chemical etching constant k_n was estimated to be 10 cm/s, and the ion-assisted etching constant k_+ was estimated to be 10^{-25} mol/eV. These values were estimated from a limited number of independent experimental data on loading [plot of inverse of etch rate *vs.* inverse of etch-
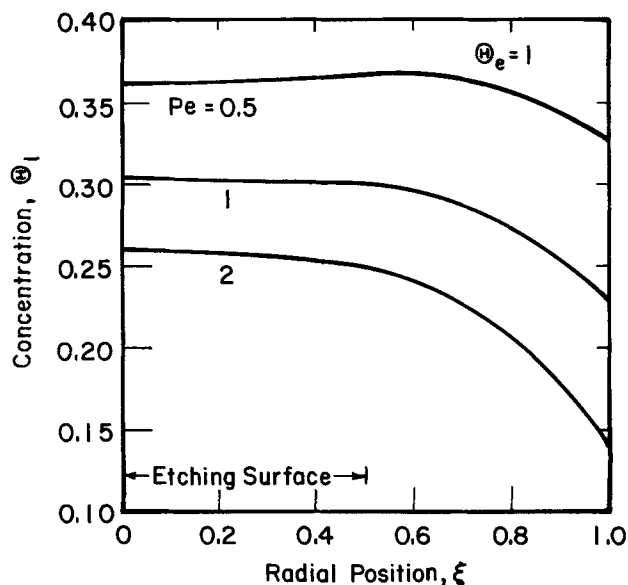
Fig. 5. Dimensionless etchant concentration as a function of radial position for different values of the Peclet number Pe. $C_0 = D_a = \Phi_0^2 = 1$, $\delta = 2$, $\gamma_2 = 0.5$, $\gamma_1 = \beta_i = 0$, $V_p^* = -50$, $\xi_1 = 0.5$, $\theta_e = 1$.

able area (28)] and etch anisotropy as measured from SEM pictures. Volume recombination rate constants (reactions [R8]-[R10] were taken as $K_1 = 2 \times 10^{15}$, $K_2 = 5 \times 10^{13}$, $K_3 = 2 \times 10^{14}$ cm^6/mol^2-s (11, 12). Wall recombination coefficients were given average values of $w_1 = 10^{-4}$ for the surface surrounding the wafer, and $w_2 = 2 \times 10^{-4}$ for the upper electrode surface (31).

Because of the uncertainty in values of key parameters, the model was used only to explore qualitative trends. Figure 6b gives calculated results for the pressure dependence of the relative etch rate, expressed as the etch rate normalized with respect to the value obtained at 1 torr pressure, 100W power, and 100 sccm gas flow rate. A decrease in pressure is accompanied by reduced molecular oxygen concentration and smaller gas residence times. These two effects more than compensate for the increase in electron temperature and density with decreasing pressure. The net result is lower etchant concentration and lower etch rates. At higher pressures volume recombination reactions become important and the etch rate increases slower with pressure. Glow stratification phenomena observed at higher pressures (> 2 torr) are not accounted for in the model.

Comparison of experimental data (Fig. 6a) with theoretical calculations (Fig. 6b) indicates that the relative change in etch rate with pressure is similar in both cases. For example, the etch rate at 2 torr is predicted to be 1.3 times that at 1 torr, in good agreement with experimental data.

Figure 7a gives experimental data on etch rate *vs.* power at two radial positions on the wafer. As power is increased, the electron density also increases, resulting in higher production rate of atomic oxygen and higher ion flux to the surface. In addition, the sheath voltage increases with a concomitant increase in ion bombardment energy. Thus both chemical and ion-assisted etching increase with power, but with sacrifice of reaction uniformity across the wafer. By comparison with calculated results of relative etch rate shown in Fig. 7b, one observes that theory represents qualitative trends relatively well. By comparison of Fig. 7a with 7b, one observes the linear increase in etch rate at low power values is represented by the model, as are relative changes in etch rate. At high power values, however, the plasma was observed to spread outside the etching chamber so that, as a consequence, the power density was less than that used for theoretical calculations. Therefore, for high power, experimental data fall below the model predictions.

Experimental data for the effect of flow on etch rate are shown in Fig. 8a for two values of pressure; these data are
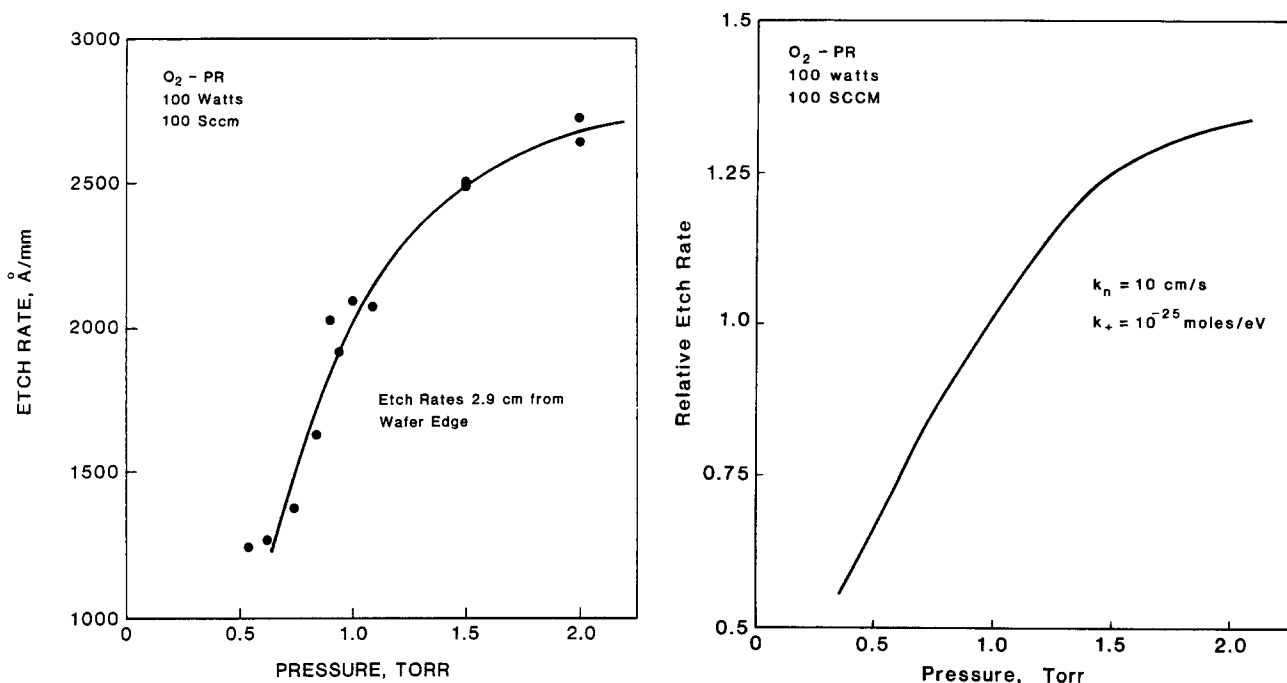
Fig. 6 (a, left) Measured photoresist etch rate as a function of reactor pressure. (b, right) Predicted average relative etch rate as a function of reactor pressure. Etch rate was normalized with respect to that at 1 torr, 100W, and 100 sccm oxygen flow.

to be compared with predictions of relative etch rate shown in Fig. 8b. Initially etch rate decreases with flow rate because convection serves to sweep away active species (see also Fig. 5 showing a decrease in concentration as Pe increases). As flow rate (Pe) increases, the average concentration in the reactor continues to decrease (though at a slower rate) but the concentration profile closer to the reactor exit becomes highly nonuniform as seen also in Fig. 5. Note that, for the situation at hand, a Pe value of 2 corresponds to flow rate of 500 sccm. Because for high flow rates, the concentration in the central part of the reactor is not significantly affected by flow, the etch rate remains essentially constant. The model captures several salient features of the experiment: the initial decrease in etch rate with flow, the insensitivity of etch rate at high flow rates, and the "turning point" at around 500 sccm.

Temperature effects have not been considered in the reactor analysis. Temperature affects the reactant concentration, the rate of electron induced reactions in the glow (by affecting E_{ef}/N at constant pressure), and the reaction rate constants. However, experimental data showed that over the range 25°-75°C of substrate electrode temperature, etch

rate was little affected by temperature. Hence, in the present case, temperature effects appear to be of secondary importance in studying etch rate changes with reactor operating variables.

Summary and Conclusions

A mathematical model has been developed for a parallel plate plasma etching reactor for the case of the oxygen discharge. The model included the variation of electron density and energy with operating conditions, the potential distribution and ion transport in the sheath, the ion-assisted reaction kinetics on the surface, and the transport and reactions of neutral and charged species.

The following approximations and assumptions were introduced in order to simplify the analysis (i) the continuum approximation is valid ($\lambda << L$); (ii) time-average quantities for potential and species concentration can be used; (iii) the glow is spatially uniform with a Maxwellian distribution of electron energies, (iv) negative ion effects can be neglected, (v) a one-dimensional radial dispersion transport model is applicable, (vi) the reactor operates isothermally and physical and transport coefficients are con-
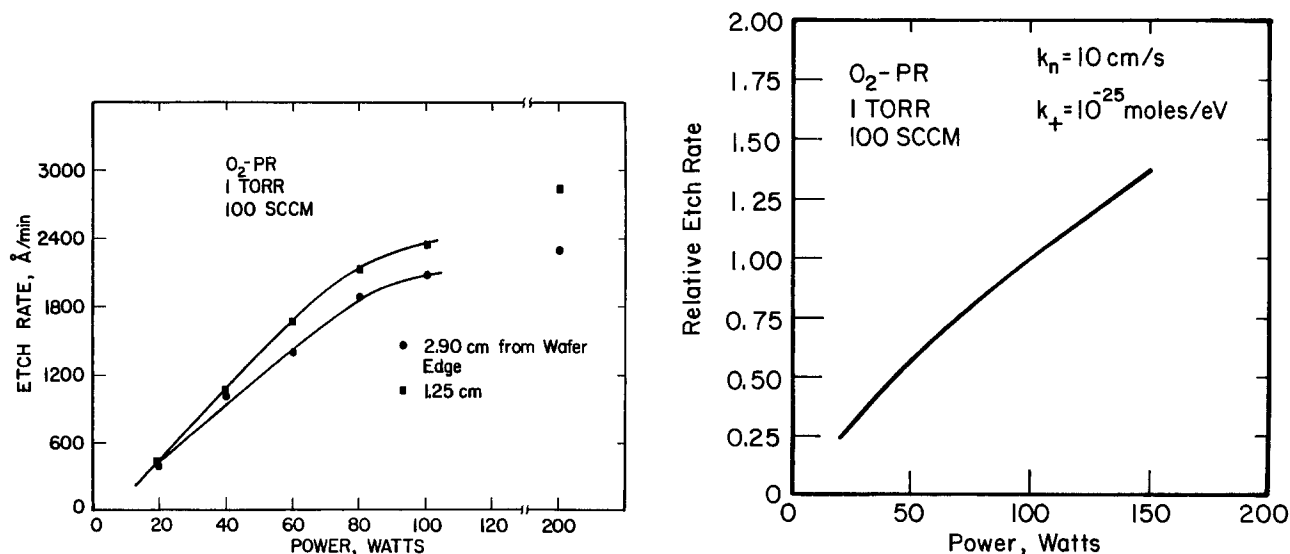
Fig. 7. (a, left) Measured photoresist etch rate as a function of power input. (b, right) Predicted average relative etch rate as a function of power input. Etch rate was normalized with respect to that at 1 torr, 100W, and 100 sccm of oxygen flow.
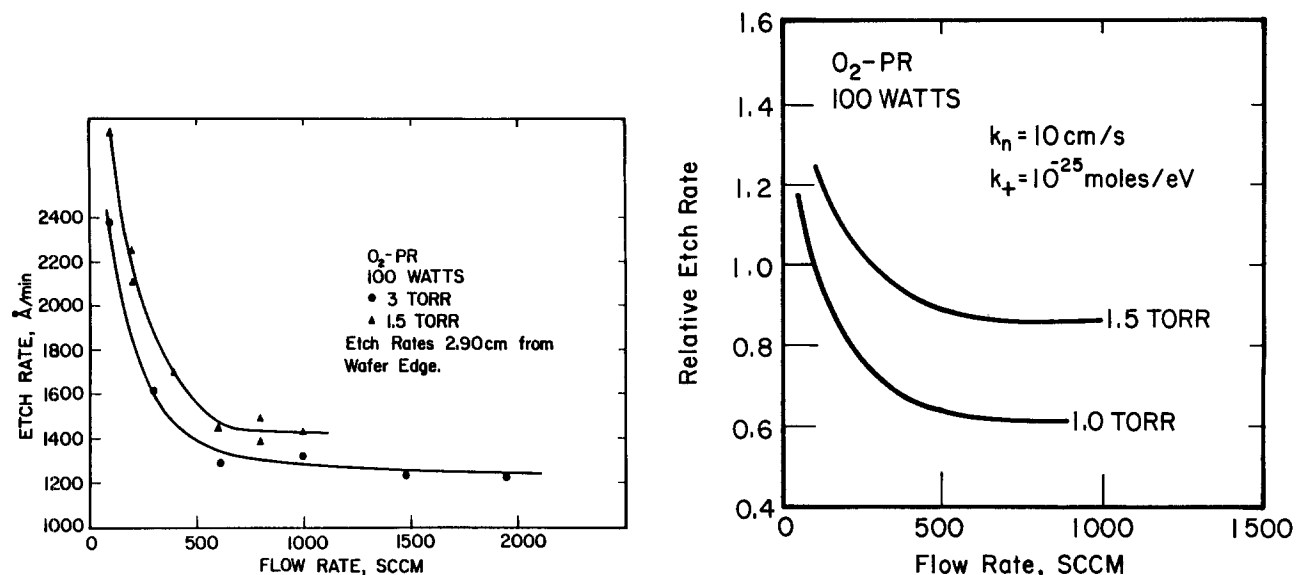
Fig. 8. (a, left) Measured photoresist etch rate as a function of flow rate. (b, right) Predicted average relative etch rate as a function of flow rate. Etch rate was normalized with respect to that at 1 torr, 100W, and 100 sccm of oxygen flow.

stant, (vii) the wafer is in good electrical and thermal contact with the substrate electrode, (viii) plasma contamination by reaction products is negligible, and (ix) the most important species are O, O_2, O_2^+, and electrons.

The model was used to predict active species concentration profiles and etch rate distribution upon variation of reactor operating conditions. Emphasis was placed on operating conditions typical of single-wafer etching. Important dimensionless variables were identified and their effect on reactor behavior was examined. The variation of etch uniformity with Thiele modulus (Φ_o^2) and Peclet number (Pe) was investigated. For uniform ion flux along the etching surface, uniform etching was predicted for $\Phi_o^2 < 1$ and for Pe close to unity. Over the parameter range examined, etch rate was predicted to increase with pressure at low pressure ($\lesssim 1$ torr) and to saturate at higher pressure. Etch rate increased almost linearly with power and decreased with flow rate (at the high flow rate regime, $Q \gtrsim 100$ sccm). At very high flow rates ($Q \gtrsim 500$ sccm) etch rate was insensitive to flow. The foregoing theoretical predictions of etch rate as a function of pressure, power, and flow rate were in good qualitative agreement with experimental data obtained by etching polymer films in an oxygen plasma in a single-wafer etcher.

The model predictions were based on a tentative kinetic expression for the ion-assisted etching and on estimated values of the etching and wall recombination rate constants. The uncertainty in the kinetic expression is not expected to have significant effect under conditions of relatively high pressure since chemical etching dominates in the high pressure oxygen plasma etching polymer. However, ion-assisted etching may be important in the low pressure regime and in other systems such as Cl_2 plasma etching of undoped silicon.

There is need for more precise information on the kinetics of etching and of other surface reactions such as recombination or polymerization. In the absence of such information, one may use a large number of experimental data on etch rate, anisotropy, and uniformity, and try different kinetic models in an effort to obtain the best fit of the data to the model predictions.

Owing to the complexity of plasma reactor systems, simplifying assumptions were introduced in order to simulate the specific experimental system under study. Two assumptions which limit the parameter range over which the model is applicable include the continuum approximation, valid only for relatively high pressure ($\gtrsim 0.25$ torr) operation, and the time-average sheath assumption, valid only for high frequencies ($\gtrsim 10$ MHz). In addition, the simplified discharge model used is based on inexact knowl-

edge and may not be accurate when secondary electron emission is important.

The strong interdependence of plasma and surface chemistry, reactor design, and operating conditions, makes the task of plasma reactor design and scale-up very challenging. The reactor engineering approach used here appears to offer a rational procedure for improving upon trial-and-error methods. When used in conjunction with well-characterized experiments, mathematical models can be useful for improving the bridge between scientific understanding and engineering design.

Acknowledgments

LIST OF SYMBOLS

An	degree of anisotropy
A_{PR}	exposed photoresist area, cm^2
C	species concentration, mol/cm^3
C_o	inlet gas concentration, mol/cm^3
Co	collision number, dimensionless
D	diffusion coefficient, cm^2/s
Da	Damköhler number, dimensionless, Eq. [19]
E	electric field, V/cm
e	electronic charge, $1.602 \ 10^{-19}$ Cb
G	generation rate, mol/cm^3-s
I	current, (cm^2-s)$^{-1}$ or mA/cm^2
K_i	volume recombination rate constant, cm^6/mol^2-s ($i = 1, 2, 3$)
k	Boltzmann constant, $1.38066 \ 10^{-23}$ J/K
k_{sub}	reaction rate constant, cm^3/s (sub refers to appropriate subscript)
k_n	chemical (neutral) etching rate constant, cm/s
k_+	ion-assisted etching rate constant, mol/eV
k_p	etchant production rate constant, cm^3/s
L	half-interelectrode gap, cm
M_1	atomic oxygen mass, g
M_2	molecular oxygen mass, g
m	electronic mass, g
n	charged particle number density in plasma, cm^{-3}
N	neutral number density, cm^{-3}
P	power, W

p	pressure, torr
Pe	Peclet number, dimensionless, Eq. [19]
Q	gas flow rate corrected for plasma reactor conditions, cm^3/s
Q_o	input gas flow rate, sccm (std cm^3/min)
R_t	total etching rate, mol/cm^2-s or Å/min
R_n	chemical etching rate, mol/cm^2-s
R_+	ion-assisted etching rate, mol/cm^2-s
R_g	gas constant, 62,358 torr-cm^3/mol-K
r	radial coordinate, cm
r_1	wafer radius, cm
r_2	reactor radius, cm
T_g	gas temperature, K
T_e	electron temperature, K
u_d	ion drift velocity, cm/s
U	radial gas velocity, cm/s
v_p	plasma volume, cm^3
V	potential, V
V_p	plasma potential, V
w_1	substrate electrode wall recombination coefficient, dimensionless
w_2	counterelectrode wall recombination coefficient, dimensionless
z	axial coordinate, cm

Greek

β_i	dimensionless groupings, Eq. [20] ($i = 1, 2, 3$)
γ_i	dimensionless groups, Eq. [20] ($i = 1, 2$)
δ	dimensionless group, Eq. [20]
ϵ_+	ion bombardment energy, eV
ζ	dimensionless axial coordinate
θ	dimensionless concentration
λ	gas mean free path, cm
λ_D	Debye length, cm
Λ	electron diffusion length, cm
ξ	dimensionless radial coordinate
σ_t	total ion-molecule collision cross section, cm^2
Φ_o^2	Thiele modulus, dimensionless, Eq. [19]

Subscripts

ex	exit conditions
R	reference value
+	positive ions
e	electrons
1	atomic oxygen
2	molecular oxygen
ef	effective
g	gas

Superscript

*	dimensionless quantity

REFERENCES

1. "VLSI Electronics: Microstructure Science," Vol. 8, N. G. Einspruch and D. M. Brown, Editors, "Plasma Processing for VLSI," Academic Press, Inc., New York (1984).
2. K. D. Allen, H. H. Sawin, M. T. Mocella, and M. W. Jenkins, *This Journal*, **133**, 2315 (1986); K. D. Alen and H. H. Sawin, *ibid.*, 2326; K. D. Allen, H. H. Sawin, and A. Yokozeki, *ibid.*, 2331.
3. M. J. Kushner, *J. Appl. Phys.*, **53**, 2923, 2939 (1982).
4. D. B. Graves and K. F. Jensen, *IEEE Trans. Plasma Sci.*, **PS-14**, 78 (1986).
5. M. Dalvie, K. F. Jensen and D. B. Graves, *Chem. Eng. Sci.*, **41**, 653, (1986).
6. D. Edelson and D. L. Flamm, *J. Appl. Phys.*, **56**, 1522 (1984).
7. L. E. Kline, *IEEE Trans. Plasma Sci.*, **PS-14**, 145 (1986).
8. R. C. Alkire and D. J. Economou, *This Journal*, **132**, 648 (1985).
9. M. Doken and I. Miyata, *ibid.*, **126**, 2235 (1979).
10. P. D. DeGraff and D. C. Flanders, *J. Vac. Sci. Technol.*, **16**, 1906 (1979).
11. J. W. Dettmer, Ph.D. Thesis, AFIT/DS/78-3, Air Force Institute of Technology (1978).
12. A. T. Bell, in "Techniques and Applications of Plasma Chemistry," J. R. Hollahan and A. T. Bell, Editors, p. 1, John Wiley & Sons, Inc., New York (1974).
13. A. T. Bell and K. Kwong, *AIChE J.*, **18**, 990 (1972).
14. B. E. Cherrington, "Gaseous Electronics and Gas Lasers," Pergamon Press, Ltd., Oxford (1980).
15. F. Kaufman, in "Chemical Reactions in Electrical Discharges," Advances in Chemistry Series, Vol. 80, p. 29, ACS Washington, DC (1969).
16. G. L. Rogoff, J. M. Kramer, and R. B. Piejak, *IEEE Trans. Plasma Sci.*, **PS-14**, 103 (1986).
17. D. Economou, D. Evans, and R. Alkire, *This Journal*, **135**, 756 (1988).
18. J. B. Thompson, *Proc. R. Soc. London Ser. A*, **262**, 503 (1961).
19. W. P. Allis and D. J. Rose, *Phys. Rev.*, **93**, 84 (1954).
20. G. F. Froment and K. B. Bischoff, "Chemical Reactor Analysis and Design," John Wiley & Sons, Inc., New York (1979).
21. U. Gerlach-Meyer, J. W. Coburn, and E. Kay, *Surf. Sci.*, **103**, 177 (1981).
22. H. F. Winters and J. W. Coburn, *J. Vac. Sci. Technol.*, **B3**, 1376 (1985).
23. Y. H. Lee and M.-M. Chen, *J. Appl. Phys.*, **54**, 5966 (1983).
24. J. F. Battey, *This Journal*, **124**, 147 (1977) and *IEEE Trans. Electron. Devices*, **ED-24**, 140 (1977).
25. J. M. Cook and B. W. Benson, *This Journal*, **130**, 2459 (1983).
26. D. M. Flamm, V. M. Donnelly, and J. A. Mucha, *J. Appl. Phys.*, **52**, 3833 (1981).
27. G. C. Schwartz, L. B. Rothman, and T. J. Schopen, *This Journal*, **126**, 464 (1979).
28. C. J. Mogab, *ibid.*, **124**, 1262 (1977).
29. A. G. Nagy, *ibid.*, **131**, 1871 (1984).
30. G. S. Selwyn, *J. Appl. Phys.*, **60**, 2771 (1986).
31. F. Kaufman, in "Progress in Reaction Kinetics," Vol. 1, G. Porter, Editor, p. 1 Pergamon Press, Inc., New York (1961).
32. B. A. Finlayson, "Nonlinear Analysis in Chemical Engineering," McGraw-Hill, New York (1980).